LBNL-0000

Lawrence Berkeley National Laboratory

Optimal sizing and placement of energy storage systems and on-load tap changer transformers in distribution networks

José Iria[a,b], Miguel Heleno[a], and Gonçalo Candoso[a]

[a] Grid Integration Group, Lawrence Berkeley National Laboratory, Berkeley, USA
[b] Centre for Power and Energy Systems, INESC TEC, Porto, Portugal

Published in Applied Energy

September 2019

Partial funding for this work was provided by the Office of Electricity, Microgrids R&D and Advanced Grid Modeling Programs, of the U.S. Department of Energy under Contract No. DE-AC02-05CH11231.

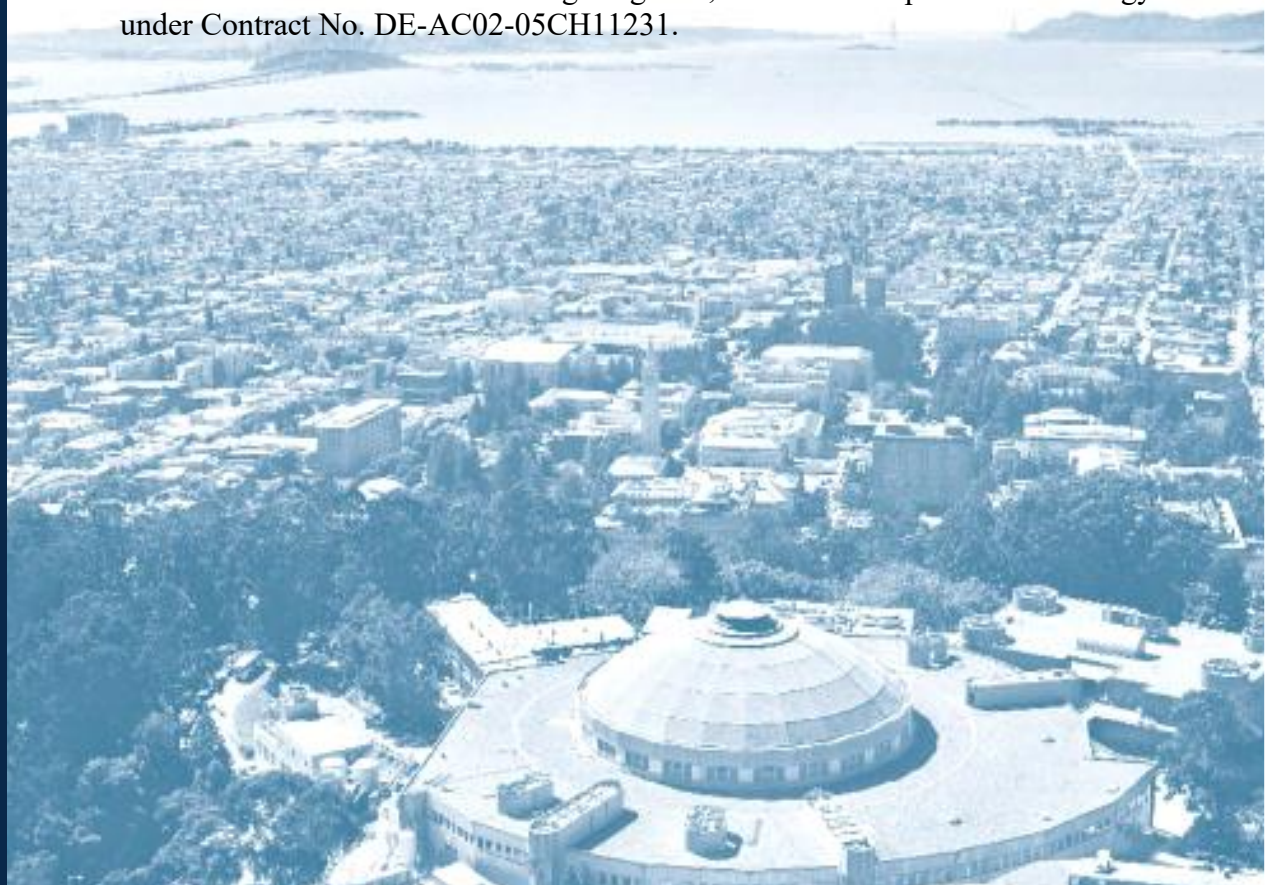

Disclaimer

Optimal sizing and placement of energy storage systems and on-load tap changer transformers in distribution networks

José Iria[a,b,*], Miguel Heleno[a], and Gonçalo Candoso[a]

[a] Grid Integration Group, Lawrence Berkeley National Laboratory, Berkeley, USA
[b] Centre for Power and Energy Systems, INESC TEC, Porto, Portugal

[*]Corresponding author. E-mail address: jpiria@inesctec.pt

Abstract

The large-scale deployment of distributed energy resources will produce reverse power flows, voltage, and congestion problems in the distribution networks. This paper proposes a novel optimization model to support distribution system operators planning future medium voltage distribution networks characterized by high penetration of behind-the-meter distributed energy resources. The optimization model defines the optimal mix, placement, and size of on-load tap charger transformers and energy storage devices with the objectives of mitigating network technical problems and minimizing both investment and operation costs. The proposed optimization model relaxes the non-convex formulation of the optimal power flow to a constrained second-order cone programming model and exactly linearizes the non-linear model of the on-load tap changer transformer via binary expansion scheme and big-M method. These two transformations reduce the computational burden of the optimization allowing it to be applicable to real-scale distribution grids, as demonstrated by the results. The numerical results also show that the joint optimization of energy storage devices and on-load tap changer transformers produces a more affordable and flexible planning strategy than the individual optimization of the technologies.

Keywords: Energy storage; on-load tap changer transformer; optimal power flow; second-order cone programming; planning.

Nomenclature

Abbreviations

DSO	distribution system operator
EV	electric vehicle
HV	high voltage
LV	low voltage
MV	medium voltage
OLTC	on-load tap changer
OPF	optimal power flow
PV	photovoltaic unit
SOCP	second-order cone programming

Indices and sets

i, j, k	buses

$(i,j) \in N^L$	collection of lines from bus i to bus j
$t \in T$	time intervals (h)
N^B	set of buses
N^O	set of buses with either existing or possible MV/LV OLTC transformers
N^S	set of candidate buses to place energy storage
$n \in N^T$	length of the binary tap representation $\{1,2,\dots\}$
n^{ref}	tap position that corresponds to 1 p.u. of turn ratio
$d \in N^D$	selected days
$T^B \subset T$	subset of periods that set the beginning of the day
$T^E \subset T$	subset of periods that set the ending of the day

Parameters

$\bar{S}$	maximum capacity of the branch (p.u.)
S^b	base power (kVA)
r	resistance (p.u.)
$\bar{I}$	maximum current (p.u.)
x	reactance (p.u.)
$\dot{\lambda}^S$	fixed investment price of energy storage (€)
$\dot{\lambda}^O$	fixed investment price of MV/LV OLTC transformer (€)
$\ddot{\lambda}^S$	variable investment price of energy storage (€/kWh)
$\ddot{\lambda}^O$	variable investment price of MV/LV OLTC transformer (€/kVA)
λ^E	energy price (€/kWh)
$\ddot{\lambda}^{\ddot{O}}$	tap changing prices of HV/MV and MV/LV OLTC transformers (€/tap)
η^+, η^-	charging, discharging efficiencies
Δt	duration of the time interval t (1 h)
$\Delta\varphi$	turn ratio change per tap (p.u.)
$\Delta\alpha$	turn ratio change associated to a binary tap position
$\underline{\varphi}, \overline{\varphi}$	minimum, maximum turn ratios (p.u.)
$\underline{\gamma}$	self-discharge rate of energy storage
$\overline{\beta^S}, \underline{\beta^S}$	maximum, minimum size of energy storage (kWh)
$\overline{\beta^O}$	size of the installed transformer without OLTC capabilities (kVA)
$\bar{\phi}$	total number of taps
ς	minimum state-of-charge
ρ	power to energy ratio of the energy storage
ψ	reactive to active power ratio of the energy storage
W	weight of the daily profile
$\bar{V}, \underline{V}$	maximum, minimum voltages (p.u.)
P^I, Q^I, S^I	inflexible active, reactive, apparent power (p.u.)
M	arbitrarily large number

Variables

I	current (p.u.)
L	squared current (p.u.)
$V, \tilde{V}$	voltage (p.u.)

$U, \widetilde{U}, \widehat{U}$	squared voltage (p.u.)
θ^S	binary investments in energy storage devices
θ^O	binary investments in MV/LV OLTC transformers
φ	turn ratio of the OLTC transformer (p.u.)
ϕ	integer tap position of the OLTC transformer
SOC	state-of-charge (kWh)
P^+, P^-	charging, discharging active power (kW)
$Q^{+/-}$	reactive power of the energy storage (kVAR)
$P^F, \widehat{P}^F$	active power flow (p.u.)
$Q^F, \widehat{Q}^F$	reactive power flow (p.u.)
δ^+, δ^-	number of tap changes in the positive, negative directions
β^S, β^O	size of energy storage (kWh), MV/LV OLTC transformer (kVA)
α	binary representation of the tap positions
m, x, y	auxiliary variables

1. Introduction

1.1. Motivation

The emission targets of Paris climate agreement will require two major transformations in the electricity sector: 1) increasing the generation from renewable energy sources at the distribution level; 2) electrifying the transportation sector, namely by replacing internal combustion engine vehicles by electric vehicles (EVs). However, this revolution at the edge of the electricity system brings new challenges to the planning and operation of distribution networks, such as reverse power flows along with voltage and congestion problems, which will require a significant upgrade of grid assets as well as optimization-based tools for economically plan and operate them. Grid-connected energy storage and on-load tap changer (OLTC) transformers will play an important role in this infrastructure upgrade, as they are flexible control mechanisms that are becoming economically competitive. Thus, the optimal placement and sizing of energy storage systems and OLTC transformers will be vital to reduce investment and operation costs of distribution system operators (DSOs).

1.2. Related work

Electricity system planning methodologies have started to consider energy storage for different purposes including frequency regulation [1], energy arbitrage [2], microgrid applications [3], voltage regulation [4], and alleviate grid congestions [5]. At the transmission level, Dvorkin *et al.* [2] proposed a bi-level optimization model to size and place an energy storage device to perform energy arbitrage. In a later work [1], the application of the energy storage was extended to the provision of frequency regulation services. In the microgrid paradigm, several optimization models under the form of mixed-integer linear problems have been proposed to size and place energy storage devices for the provision of multiple services, such as energy arbitrage [6,7], peak shaving, and reliability services to ensure the safe operation of the microgrid in grid-connected and islanded modes [8]. At medium voltage (MV) distribution level, planning methodologies consider energy storage as an instrument to perform voltage regulation [4,9] and alleviate network congestions [5,10]. Yang *et al.* [9] presented a heuristic based on power flows to size energy storage, while Alnaser *et al.* [5] addressed the same

problem by presenting an optimization model with the non-convex formulation of the optimal power flow (OPF). Both works are exclusively focused on the sizing problem. Placement involves representing the network constraints, which has been addressed by other authors either using second-order cone programming (SOCP) [10,11], metaheuristics [4] or linear models [12,13]. Placement and sizing were simultaneously addressed in [14,15] with optimization models based on the SOCP-OPF. In fact, as discussed in previous works [16,17], the OPF relaxation via SOCP convexifies the power flow equations, allowing the OPF model to be applicable to large-scale problems.

OLTC transformers have been traditionally used by DSOs to automatically control voltages at the HV/MV substations [18,19]. However, the installation of OLTC at the MV/LV transformer is becoming more common with the increasing adoption of distributed energy resources by low voltage (LV) consumers. This can be seen in recent studies considering OLTC transformers in distribution network planning and operation [20,21]. Armendáriz *et al*. [20] proposed a network optimization model to place MV/LV OLTC transformers and later [21] the author presented a coordinated planning strategy to demonstrate the benefit of OLTC transformer investments in microgrid/utility boundary locations. Hosseinpour and Bastaee [22] included network equations and solved the problem of OLTC transformer placement, applying the non-convex formulation of the OPF, while using a metaheuristic to solve the non-linear problem. In a later work, Xie *et al.* [23] solved the problem of optimal placement of OLTC transformers using SOCP-OPF.

1.3. Contributions

This paper proposes a novel optimization model to support DSOs in the planning of MV distribution networks. The aim is to improve the network operation and mitigate possible network problems, such as undervoltages and overvoltages that may arise from the high integration of distributed energy resources at the LV level. Two smart grid technologies are considered in the planning problem: energy storage devices to perform energy arbitrage and voltage regulation; and OLTC transformers to perform voltage regulation.

The proposed optimization model defines the optimal mix, placement, and sizing of energy storage devices and MV/LV OLTC transformers that mitigate network technical problems and minimize overall investment and operation costs. Investment costs include fixed and variable components of new energy storage devices and MV/LV OLTC transformer installations while operation costs include network energy losses, energy storage arbitrage and tap changes of OLTC transformers located at HV/MV and MV/LV substations. The non-convex formulation of the OPF is relaxed to a constrained SOCP model, while the non-linear OLTC model is exactly linearized via binary expansion scheme and big-M method. These two transformations make the optimization problem solvable via mixed-integer quadratically constrained programming.

In the scope of distribution network planning, the proposed optimization model improves the state-of-the-art in the following points:

1. it considers the joint sizing and placement of energy storage devices and MV/LV OLTC transformers, which differs from approaches only focused on energy storage devices [9,14] or OLTC transformers [20,21]. The joint optimization of these two technologies produces a more affordable planning strategy than the

individual optimization of the technologies, as shown in the results section. To the authors' knowledge, no paper in the literature has presented an optimization formulation targeting planning problems that simultaneously consider OLTC transformers and energy storage devices;

2. it exploits a SOCP-OPF model constrained by the *LinDistFlow* formulation [24] to ensure that the OPF solutions have physical meaning for extreme scenarios of network operation characterized by undervoltages and overvoltages. The solutions of the classic SOCP-OPF [15] may lose physical meaning in the mentioned scenarios, as discussed in [25]. This paper analyzes scenarios of undervoltages, overvoltages, and reverse power flows;
3. it is applicable to real-scale MV distribution grids, as demonstrated in the results section for a 118-bus test system. Alternative approaches to real-scale distribution grids exploit linear OPF models [12,13] and metaheuristics [4,22]**.** However, the linear models and metaheuristics present drawbacks. The metaheuristics do not ensure the global optimality of the OPF problem and the linear models may produce technically infeasible solutions, as shown in the results section.

In short, the proposed optimization model improves the planning of real-scale MV distribution grids by defining a more affordable and flexible plan for the placement and sizing of energy storage devices and MV/LV OLTC transformers.

1.4. Paper organization

The remaining paper is organized as follows: section 2 reviews the non-convex formulation of the OPF for distribution grids with OLTC transformers; sections 3 and 4 present the methodology for the optimal sizing and placement of energy storage devices and OLTC transformers; the case study and results are described in sections 5 and 6; section 7 is the conclusion.

2. Non-convex formulation of the optimal power flow for radial distribution networks

This section reviews the non-convex formulation of the OPF for radial networks with OLTC transformers.

2.1. Branch flow model for radial networks

The non-convex formulation of the OPF in the form of branch flow is formulated in equations (1)-(7) [24]. The objective function (1) minimizes the energy network losses.

$$Min \sum_{(i,j)\in\beta} r_{i,j} I_{i,j}^2 \tag{1}$$

The first two constraints (2) and (3) set the active $P_{i,j}^F$ and reactive $Q_{i,j}^F$ power flows between buses i and j. The parameters are the inflexible active power P_j^I, inflexible reactive power Q_j^I, resistance $r_{i,j}$ and reactance $x_{i,j}$. The variable I is the current between buses. The inflexible power is positive for load and negative for generation. Note that the buses i, j, k are oriented as described in Figure 1.

$$P_{i,j}^F = P_j^I + \sum_{k:j\to k} P_{j,k}^F + r_{i,j} I_{i,j}^2, \qquad \forall\,(i,j) \in N^L \tag{2}$$

$$Q_{i,j}^F = Q_j^I + \sum_{k:j\to k} Q_{j,k}^F + x_{i,j} I_{i,j}^2, \qquad \forall\,(i,j) \in N^L \tag{3}$$

Constraints (4) and (5) define the voltage in each bus $j \in N^B$ and its limits $\left[\underline{V_j}, \bar{V}_j\right]$. The slack bus is represented by bus 0 and the voltage is fixed. Constraints (6) and (7) set the current and the ampacity limits $\bar{I}_{i,j}$ of the branches.

$$V_j^2 = V_i^2 - 2\left(r_{i,j} P_{i,j}^F + x_{i,j} Q_{i,j}^F\right) + \left(r_{i,j}^2 + x_{i,j}^2\right) I_{i,j}^2, \qquad \forall\,(i,j) \in N^L \tag{4}$$

$$\underline{V_j} \le V_j \le \bar{V}_j, \qquad \forall\ j \in N^B \tag{5}$$

$$I_{i,j}^2 V_i^2 = {P_{i,j}^F}^2 + {Q_{i,j}^F}^2, \qquad \forall\,(i,j) \in N^L \tag{6}$$

$$0 \le I_{i,j} \le \bar{I}_{i,j}, \qquad \forall\,(i,j) \in N^L \tag{7}$$

This optimization problem is non-convex. However, it can be relaxed to a convex problem using second-order cone constraints. Section 3 presents a constrained SOCP-OPF.

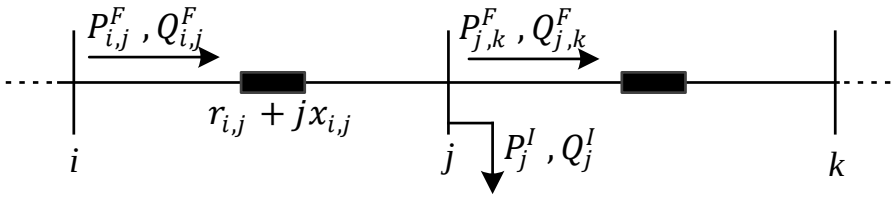

Figure 1. Representation of one feeder.

2.2. On-load tap changer transformer model

The introduction of HV/MV and MV/LV OLTC transformers into the OPF model requires replacing one existing constraint and adding four new ones. In this case, constraint (5) is replaced by constraint (8) to exclude buses with OLTC transformers.

$$\underline{V_j} \le V_j \le \bar{V}_j, \qquad \forall\ j \in N^B \backslash \{N^O\} \tag{8}$$

Constraints (9)-(12) are added to the initial formulation. Constraint (9) sets the voltage on the MV side of the network. The voltage $\tilde{V}_j$ is fixed (e.g., 1 p.u.) if the bus has an HV/MV OLTC transformer (i.e., slack bus). In case of the bus having a MV/LV OLTC transformer, the variable $\tilde{V}_j$ defines the voltage in the secondary side of the transformer. Constraint (10) defines the turn ratio φ_j of the OLTC transformer. The parameters $\underline{\varphi_j}$ and $\Delta\varphi_j$ are the minimum turn ratio and turn ratio change per tap, respectively. The integer variable ϕ_j represents the actual tap position of the OLTC. Constraint (11) limits the tap positions $\left[0, \overline{\phi_j}\right]$. Constraint (12) ensures the voltage limits in the secondary side of the transformer.

$$V_j = \tilde{V}_j \varphi_j, \qquad \forall\, j \in N^O \tag{9}$$

$$\varphi_j = \underline{\varphi_j} + \Delta\varphi_j \cdot \phi_j, \qquad \forall\, j \in N^O \tag{10}$$

$$0 \le \phi_j \le \overline{\phi_j}, \qquad \forall\, j \in N^O \tag{11}$$

$$\underline{V_j} \le \tilde{V}_j \le \bar{V}_j, \qquad \forall\, j \in N^O \tag{12}$$

The OLTC model (9)-(12) is non-linear. However, it can be transformed into a set of mixed integer linear constraints via binary expansion scheme and big-M method. Section 3 presents an exact linearization of the OLTC transformer model incorporated into the constrained SOCP-OPF.

3. Optimization model for sizing and placement of energy storage devices and on-load tap changer transformers

The aim of this optimization model is to support DSOs in the planning of the MV distribution networks. The model defines the optimal mix, size, and placement of energy storage devices and MV/LV OLTC transformers in MV distribution networks by minimizing the overall investment and operation costs. The investment costs include the placement and sizing of energy storage devices and MV/LV OLTC transformers. The operation costs consider energy network losses and costs associated with the coordinated management of energy storage devices and OLTC transformers located and placed at the HV/MV and MV/LV substations.

3.1. Time horizon

The optimization horizon $t \in T$ covers the period of 1 year and is modeled by design-days and critical-days. The design-days model typical conditions of operation. The critical-days model extreme scenarios of operation characterized by overvoltages and undervoltages. The total investment and operation costs are annualized. The investment costs are annualized based on the expected lifetime of the technologies.

3.2. Objective function

The optimization model is formulated as a minimization problem. The objective function (13) minimizes the annualized costs of sizing, placing and operating the energy storage devices, OLTC transformers and distribution network. The objective function (13) can be divided into the following terms:

1. **investment cost terms:** the first two terms $\theta_j^S \dot{\lambda}^S + \beta_j^S \ddot{\lambda}^S$ and $\theta_j^O \dot{\lambda}^O + \beta_j^O \ddot{\lambda}^O$ represent the annualized investment costs, i.e., the fixed and variable annualized costs of installing energy storage devices and MV/LV OLTC transformers. Specifically, $\theta_j^S \dot{\lambda}^S$ and $\theta_j^O \dot{\lambda}^O$ represent the fixed costs of placing energy storage devices and MV/LV OLTC transformers in a given location, while the $\beta_j^S \ddot{\lambda}^S$ and $\beta_j^O \ddot{\lambda}^O$ are the variable costs associated with the technology size. The binary variables θ_j^S and θ_j^O represent the investment decision in each node j, while the continuous variables β_j^S and β_j^O define the size of the devices. The fixed and variable cost components are given by $\dot{\lambda}^S, \dot{\lambda}^O, \ddot{\lambda}^S$ and $\ddot{\lambda}^O$;

2. **operation cost terms:** the last three terms model the annual operating costs associated with network energy losses $\lambda_t^E r_{i,j} L_{t,i,j} S^b$, energy storage arbitrage, $\lambda_t^E P_{t,j}^+ - \lambda_t^E P_{t,j}^-$, and tap changes of HV/MV and MV/LV OLTC transformers, $\left(\delta_{t,j}^+ + \delta_{t,j}^-\right)\ddot{\lambda}_j^O$. This formulation assumes that the DSO can use energy storage devices to buy and sell energy at wholesale prices λ_t^E. Here, S^b is the base apparent power, Δt is the time step and the tap changing price is described by $\ddot{\lambda}_j^O$. Variables

in this part of the formulation include the squared current $L_{t,i,j}$, charging power $P_{t,j}^{+}$, discharging power $P_{t,j}^{-}$, and number of tap changes in the positive $\delta_{t,j}^{+}$ and negative $\delta_{t,j}^{-}$ directions.

$$\begin{aligned} Min \quad & \left[\sum_{j\in N^S}\left(\theta_j^S \dot{\lambda}^S + \beta_j^S \ddot{\lambda}^S\right) + \sum_{j\in N^O\setminus\{0\}}\left(\theta_j^O \dot{\lambda}^O + \beta_j^O \ddot{\lambda}^O\right)\right] \\ & + \left[\sum_{t\in T} W_t \left(\sum_{(i,j)\in\beta} \lambda_t^E r_{i,j} L_{t,i,j} S^b + \sum_{j\in N^S}\left(\lambda_t^E P_{t,j}^{+} - \lambda_t^E P_{t,j}^{-}\right)\Delta t \right.\right. \\ & \left.\left. + \sum_{j\in N^O}\left(\delta_{t,j}^{+} + \delta_{t,j}^{-}\right)\ddot{\lambda}_j^O\right)\right] \end{aligned} \tag{13}$$

The HV/MV substation is the slack bus and has an OLTC transformer. The candidate buses for placing energy storage devices $j \in N^S$ and MV/LV OLTC transformers $j \in N^O$ are selected by the DSO. The parameter W_t weights critical-days and design-days.

3.3. Energy storage constraints

The sizing of energy storage consists of defining the energy capacity/size β_j^S. Constraint (14) bounds the size of the energy storage $\left[\underline{\beta^S}, \overline{\beta^S}\right]$ when placed θ_j^S in node j.

$$\underline{\beta^S}\theta_j^S \le \beta_j^S \le \theta_j^S \overline{\beta^S}, \qquad \forall\, j \in N^S \tag{14}$$

Storage operation is defined by constraints (15)-(20). Constraints (15) and (16) set the range of the charging $P_{t,j}^{+}$ and discharging $P_{t,j}^{-}$ active power $\left[0, \beta_j^S \rho\right]$. The parameter ρ is the ratio between charging/discharging active power and storage's size. Constraint (17) defines the range of the reactive power $Q_{t,j}^{+/-}$ capable of being absorbed and injected by the power electronic converter connected to the energy storage. The parameter ψ defines the ratio between the reactive power and active power.

$$P_{t,j}^{-} + P_{t,j}^{+} \le \beta_j^S \rho, \qquad \forall\, t \in T,\ j \in N^S \tag{15}$$

$$P_{t,j}^{-}, P_{t,j}^{+} \ge 0, \qquad \forall\, t \in T,\ j \in N^S \tag{16}$$

$$-\psi \cdot \beta_j^S \cdot \rho \le Q_{t,j}^{+/-} \le \psi \cdot \beta_j^S \cdot \rho, \qquad \forall\, t \in T,\ j \in N^S \tag{17}$$

Constraints (18) and (19) set and bound the state-of-charge SOC. The parameters η^{+} and η^{-} are the efficiencies of the charging and discharging processes, γ is the rate of self-discharge and ς is the minimum SOC level. Constraint (20) imposes the SOC at the end of the day T_d^E equal to the SOC at the beginning of the day T_d^B. The index d defines the day.

$$SOC_{t+1,j} = SOC_{t,j}(1-\gamma) + \Delta t\left(P_{t,j}^{+}\eta^{+} - \frac{P_{t,j}^{-}}{\eta^{-}}\right), \qquad \forall\, t \in T,\ j \in N^S \tag{18}$$

$$\beta_j^S \varsigma \le SOC_{t+1,j} \le \beta_j^S, \qquad \forall\, t \in T,\ j \in N^S \tag{19}$$

$$SOC_{T_d^B,j} = SOC_{T_d^E,j}, \qquad \forall\, d \in N^D,\ j \in N^S \tag{20}$$

3.4. Radial network constraints

In this model, we relax the branch flow equations for radial networks (2)-(7) using second-order cones [25]. This is done by replacing I^2 and V^2 with the variables L and U, respectively, and by transforming the equality constraint (6) into the inequality constraint (25). These result in the relaxed SOCP model given by equations (21)-(25).

$$P^F_{t,i,j} = P^I_{t,j} + \frac{P^+_{t,j} - P^-_{t,j}}{S^b} + \sum_{k:j\to k} P^F_{t,j,k} + r_{i,j}L_{t,i,j}, \qquad \forall\, t \in T,\ (i,j) \in N^L \tag{21}$$

$$Q^F_{t,i,j} = Q^I_{t,j} + \frac{Q^{+/-}_{t,j}}{S^b} + \sum_{k:j\to k} Q^F_{t,j,k} + x_{i,j}L_{t,i,j}, \qquad \forall\, t \in T,\ (i,j) \in N^L \tag{22}$$

$$U_{t,j} = U_{t,i} - 2\left(r_{i,j}P^F_{t,i,j} + x_{i,j}Q^F_{t,i,j}\right) + \left(r^2_{i,j} + x^2_{i,j}\right)L_{t,i,j}, \quad \forall\, t \in T,\ (i,j) \in N^L \tag{23}$$

$$\underline{V_j}^2 \le U_{t,j} \le \overline{V}_j^2, \qquad \forall\, t \in T,\ j \in N^B \backslash \{N^O\} \tag{24}$$

$$L_{t,i,j}U_{t,i} \ge \left(P^F_{t,i,j}\right)^2 + \left(Q^F_{t,i,j}\right)^2, \qquad \forall\, t \in T,\ (i,j) \in N^L \tag{25}$$

The OPF problem is now convex. However, this formulation may often lead to solutions that do not satisfy the original constraint (6), i.e. to solutions that do not have physical meaning, as discussed in [25]. This may happen in extreme scenarios of network operation characterized by high voltages close to the upper-bounds of the buses. To ensure solutions with physical meaning, we define a set of ancillary variables $\{\hat{U}, \hat{P}^F, \hat{Q}^F\}$ and constraints (26)-(28) derived from the *LinDistFlow* formulation [24]. Constraints (26)-(28) upper-bound the voltages of the SOCP-OPF model. Constraint (26) forces the slack bus voltage levels in both non-linear and linear models to be equal, connecting the SOCP model to the *LinDistFlow* model. Constraint $U_{t,j} \le \overline{V}_j^2$ in (24) becomes redundant after imposing (28) since $\hat{U}_{t,j} \ge U_{t,j}$.

$$U_{t,0} = \hat{U}_{t,0}, \qquad \forall\, t \in T \tag{26}$$

$$\hat{U}_{t,j} = \hat{U}_{t,i} - 2\left(r_{i,j}\hat{P}^F_{t,i,j} + x_{i,j}\hat{Q}^F_{t,i,j}\right), \qquad \forall\, t \in T,\ (i,j) \in N^L \tag{27}$$

$$\hat{U}_{t,j} \le \overline{V}_j^2, \qquad \forall\, t \in T,\ j \in N^B \backslash \{N^O\} \tag{28}$$

The power flow variables of the *LinDistFlow* formulation $\hat{P}^F_{t,i,j}$ and $\hat{Q}^F_{t,i,j}$ denote the sum of the power injections at the buses downstream node j (inclusive). Figure 2 illustrates the calculation of variables $\hat{P}^F_{t,i,j}$ and $\hat{Q}^F_{t,i,j}$.

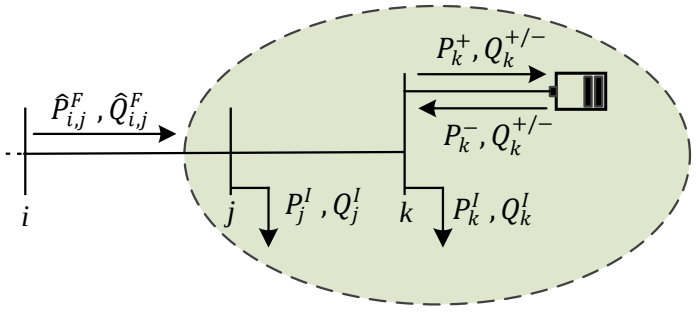

$$\hat{P}^F_{i,j} = P^I_j + P^I_k + \frac{P^+_k - P^-_k}{S^b} \qquad \hat{Q}^F_{i,j} = Q^I_j + Q^I_k + \frac{Q^{+/-}_k}{S^b}$$

Figure 2. Illustration of $\hat{P}^F_{t,i,j}$ and $\hat{Q}^F_{t,i,j}$. The shaded region contains all power injections downstream node j (inclusive).

The constrained SOCP-OPF (21)-(28) reduces the feasibility space of the OPF, eliminating points close to the voltage upper limits. However, this conservative approach guarantees that all solutions have physical meaning.

3.5. On-load tap changer transformer constraints

The non-linear OLTC model (9)-(12) is exactly linearized via a binary expansion scheme and big-M method. The turn ratio $\varphi_{t,j}$ of the OLTC transformer can be represented by the binary expansion scheme (29)-(30). The parameter $\Delta\alpha_{j,n}$ represents the turn ratio change enabled by each binary variable $\alpha_{t,j,n}$. The length of the binary representation is defined by $n \in N_j^T$. Constraint (30) ensures that the OLTC only has one tap position activated. This binary representation replaces the former formulation given by equations (10)-(11).

$$\varphi_{t,j} = \underline{\varphi_j} + \sum_{n \in N_j^T} \alpha_{t,j,n} \cdot \Delta\alpha_{j,n}, \qquad \forall\, t \in T, j \in N^O \tag{29}$$

$$\sum_{n \in N_j^T} \alpha_{t,j,n} \leq 1, \qquad \forall\, t \in T, j \in N^O \tag{30}$$

The squared voltage $U_{t,j}$ in the buses with OLTC transformers is defined by equation (31). The variable $\widetilde{U}_{t,j}$ represents $\left(\tilde{V}_{t,j}\right)^2$ and is bounded by $\left[\underline{V_j}^2, \overline{V_j}^2\right]$.

$$U_{t,j} = \widetilde{U}_{t,j}\varphi_{t,j}^2, \qquad \forall\, t \in T, j \in N^O \tag{31}$$

$$\underline{V_j}^2 \leq \widetilde{U}_{t,j} \leq \overline{V_j}^2, \qquad \forall\, t \in T, j \in N^O \tag{32}$$

Constraint (31) is non-linear and makes the problem non-convex. This nonlinearity can be addressed by applying the big-M method twice. Constraints (33)-(38) replace constraints (29) and (31). Constraint (34) results from multiplying both sides of the equation (29) by $\widetilde{U}_{t,j}$. On the other hand, constraint (33) is obtained by multiplying both sides of the equation (29) by $m_{t,j}$. Three new variables are defined $m_{t,j} = \widetilde{U}_{t,j}\varphi_{t,j}$, $y_{t,j,n} = \alpha_{t,j,n}m_{t,j}$ and $x_{t,j,n} = \widetilde{U}_{t,j}\alpha_{t,j,n}$. Constraints (35)-(38) exactly linearize variables $m_{t,j}$, $y_{t,j,n}$ and $x_{t,j,n}$ using a big-M.

$$U_{t,j} = \underline{\varphi_j} m_{t,j} + \sum_{n \in N_j^T} y_{t,j,n} \cdot \Delta\alpha_{j,n}, \qquad \forall\, t \in T, j \in N^O \tag{33}$$

$$m_{t,j} = \underline{\varphi_j}\widetilde{U}_{t,j} + \sum_{n \in N_j^T} x_{t,j,n} \cdot \Delta\alpha_{j,n}, \qquad \forall\, t \in T, j \in N^O \tag{34}$$

$$0 \leq \widetilde{U}_{t,j} - x_{t,j,n} \leq \left(1 - \alpha_{t,j,n}\right)M, \qquad \forall\, t \in T,\ j \in N^O, n \in N_j^T \tag{35}$$

$$0 \leq x_{t,j,n} \leq \alpha_{t,j,n}M, \qquad \forall\, t \in T,\ j \in N^O, n \in N_j^T \tag{36}$$

$$0 \leq m_{t,j} - y_{t,j,n} \leq \left(1 - \alpha_{t,j,n}\right)M, \qquad \forall\, t \in T,\ j \in N^O, n \in N_j^T \tag{37}$$

$$0 \leq y_{t,j,n} \leq \alpha_{t,j,n}M, \qquad \forall\, t \in T,\ j \in N^O, n \in N_j^T \tag{38}$$

Now, the OLTC model is represented by the mixed integer linear constraints (30), (32)-(38). This model is applied to HV/MV and MV/LV OLTC transformers.

The number of tap changes of the OLTC transformers is computed by constraint (39).

$$\delta_{t,j}^{+} - \delta_{t,j}^{-} = \sum_{n \in N_j^T} \left(\alpha_{t,j,n} - \alpha_{t-1,j,n}\right) n\,, \qquad \forall\, t \in T, j \in N^O \tag{39}$$

$$\delta_{t,j}^{+}, \delta_{t,j}^{-} \geq 0, \qquad \forall\, t \in T, j \in N^O \tag{40}$$

The sizing and placement of MV/LV OLTC transformers require two additional constraints (41) and (42). Constraint (41) defines the size of the MV/LV OLTC transformers based on the maximum capacity $\overline{\beta_j^O}$ of the existing transformer and on the peak apparent power $S_{t,j}^I$ from the LV side. Constraint (42) defines the placement, setting the transformer turn ratio to 1 p.u. when no OLTC is placed $\left(\theta_j^O = 0\right)$. The index n^{ref} corresponds to the binary position of the OLTC when the turn ratio equals to 1 p.u. Note that the number of taps is predefined.

$$\beta_j^O \geq \theta_j^O \max\left[\max_{t \in T}\left(S^b \cdot S_{t,j}^I\right), \overline{\beta_j^O}\right], \qquad \forall\, j \in N^O \backslash \{0\} \tag{41}$$

$$\alpha_{t,j,n^{ref}} \geq 1 - \theta_j^O, \qquad \forall\, t \in T, j \in N^O \backslash \{0\} \tag{42}$$

Constraint (43) ensures the physical meaning of the SOCP-OPF, both when MV/LV OLTC transformers are placed or not.

$$\widehat{U}_{j,t} \leq \overline{V}_j^2 \left(1 - \theta_j^O\right) + \theta_j^O \overline{\varphi}_j^2 \overline{V}_j^2, \qquad \forall\, t \in T, j \in N^O \backslash \{0\} \tag{43}$$

The full formulation of the optimization model proposed in this work is given by equations (13)-(28), (30), (32)-(43). This formulation is solvable via mixed-integer quadratically constrained programming.

4. Candidate buses, critical-days, and design-days

4.1. Candidate buses

Part of the candidate buses to place energy storage devices and MV/LV OLTC transformers can be manually selected by the DSO based on decision constraints. However, even with this pre-selection, the planning problem can end up with hundreds of candidate buses for each technology penalizing the computational efficiency of the optimization problem. Thus, the authors propose a heuristic method to reduce the candidate buses based on selective power flow evaluations that explore the control space of the HV/MV OLTC transformer. The reduction of the number of candidate buses reduces the size of the optimization problem in terms of variables and constraints, and consequently the computational time without affecting the quality of the planning solution. This reduction also makes the optimization problem feasible and scalable for real-scale distribution networks.

The sequential steps of the heuristic algorithm are presented in Figure 3. The heuristic algorithm identifies candidate buses by running a series of power flows for the entire control space of the HV/MV OLTC. Candidates buses are those with undervoltage and overvoltage problems that the HV/MV OLTC cannot solve. The heuristic algorithm is repeated for each hour of the analyzed period (e.g., 1 year).

4.2. Critical-days

The critical-days represent net-load profiles of 24 h and are selected based on the results of the heuristic algorithm. The days with the highest overvoltage or undervoltage per bus are considered critical-days. The weight of each critical-day is 1.

4.3. Design-days

The design-days represent average net-load profiles of 24 h and model typical conditions of operation. The weight of each design-day is defined by the number of design-days. For instance, if the DSO sets the number of design-days equal to 1, the weight of the design-day is 365 – nº of critical-days. In this case, the design-day is represented by an average annual net-load profile of 24 h.

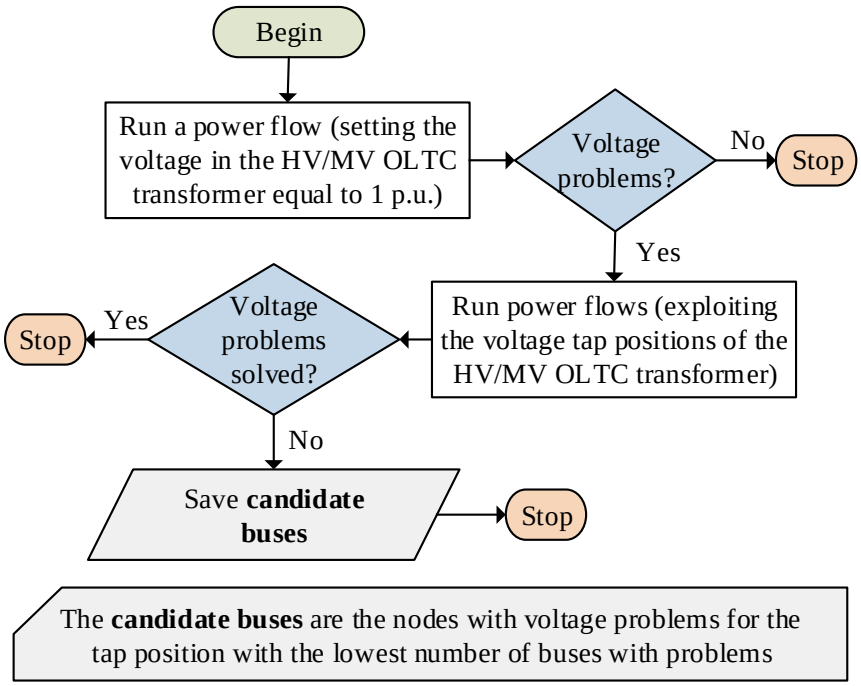

Figure 3. Flowchart of the heuristic algorithm.

5. Case study

5.1. General description

The proposed optimization model is tested using the MV distribution network described in Figure 4. Two scenarios of integration of distributed energy resources are evaluated:

1. **scenario 1**: considers the integration of 14,937 EVs in Area 2 (see Figure 4). It is assumed that 50% of the consumers in Area 2 have one EV. The EVs are not controlled by any market agent or DSO.
2. **scenario 2**: considers the integration of 59 MWp of photovoltaic units (PVs) in Area 1. It is assumed that each consumer in Area 1 has 1 PV with a peak power between 1 and 2 kWp.

5.2. Network data

The 11-kV distribution network has 118 buses, 117 branches, 1 HV/MV OLTC transformer and 117 loads. The resistance r and reactance x of the branches can be found in [26]. The bounds of the voltage magnitudes are 0.9 and 1.1 p.u. The loads are divided into three types and their main characteristics are described in Table 1. The annual hourly profiles were taken from an urban residential area in Portugal. The profiles define the base load of the system.

Table 1. Main characteristics of the loads.

Loads	Peak (kW)	Annual energy (MWh)	Transformer (kVA)	Nº of clients	Nº of loads
Profile 1	142	522	630	224	71
Profile 2	582	1975	1260	678	22
Profile 2	898	2829	1260	998	24

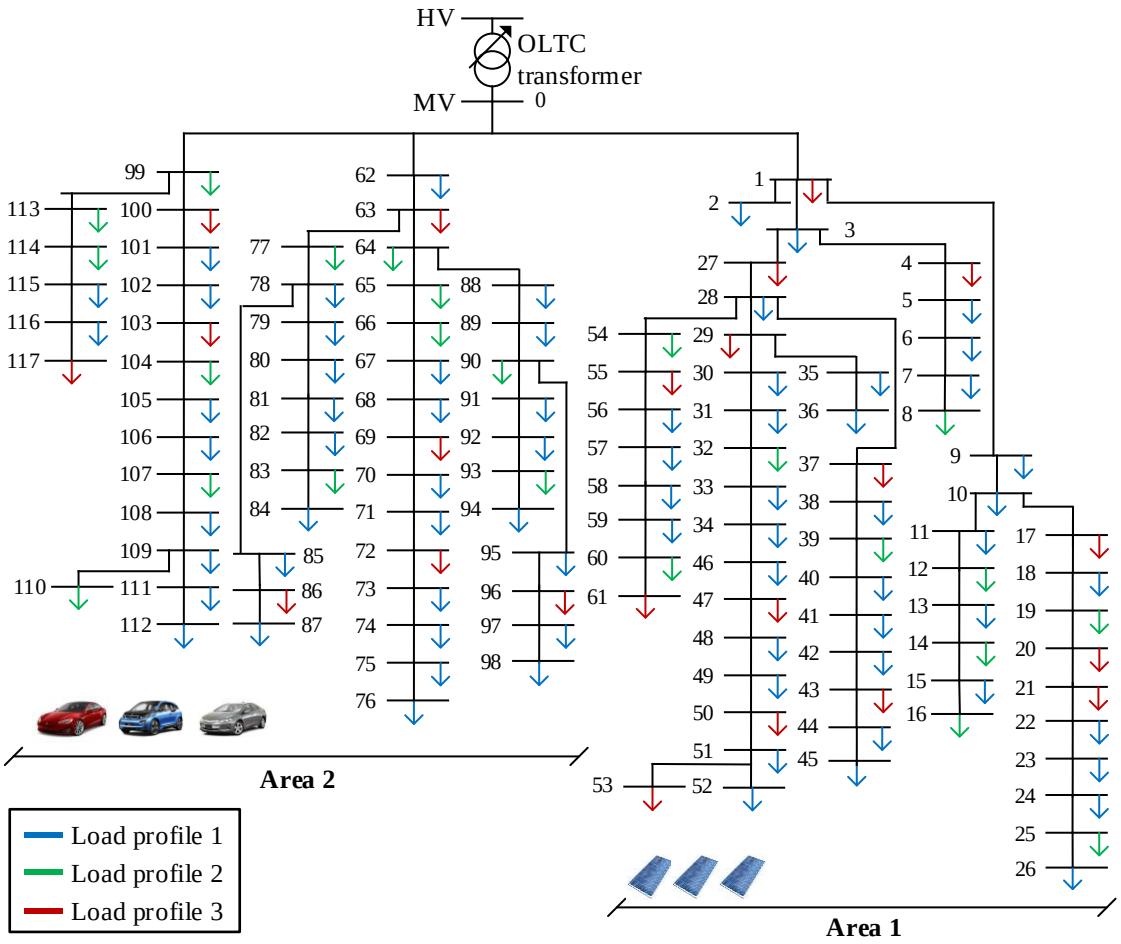

Figure 4. Medium voltage distribution network of 118 buses.

5.3. Charging profiles of the electric vehicles

The charging profiles of the EVs were computed by a discrete-time-space Markov chain [27]. This method uses traffic patterns from a residential area of the northern region of Portugal to generate the individual charging profile of each EV for the period of 1 year. The EV profiles were distributed by the network nodes of Area 2 in scenario 1, according to the ratio of 0.5 EV/client. Figure 5 illustrates the aggregated charging profile of 112 EVs located at bus 75. The load profile suggests that the EVs usually start charging at night (between the 18th and 21st hours) after the drivers arrive at home.

5.4. Photovoltaic generation profiles

The annual PV profiles were generated based on data collected from a set of generation units located in the northern region of Portugal [28]. In scenario 2, each client

of Area 1 has 1 PV with a peak power that can range from 1 to 2 kWp. Figure 5 illustrates the aggregated generation profile of 224 PVs located at bus 45.

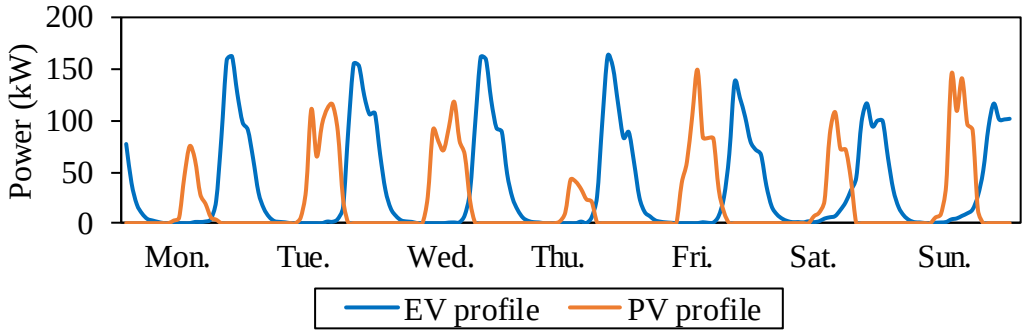

Figure 5. EV profile of bus 75 and PV profile of bus 45 for an illustrative week.

All the load and generation profiles of the electricity network can be provided upon request.

5.5. Energy storage and on-load tap changer transformers

Table 2 presents the investment and operation prices of energy storage devices, HV/MV and MV/LV OLTC transformers [21,29,30]. In the optimization model, the investment prices $\dot{\lambda}^{S}$, $\dot{\lambda}^{O}$, $\ddot{\lambda}^{S}$, $\ddot{\lambda}^{O}$ are annualized, based on the expected lifetime of the technologies. The operation prices include tap change prices $\ddot{\lambda}^{O}$ and Iberian wholesale prices λ^{E} collected from the ENTSO-E Transparency Platform [30,31]. The energy absorbed and injected by the energy storage devices is valued at wholesale prices.

Table 2. Investment and operation prices of energy storage systems and OLTC transformers.

	Energy storage	MV/LV OLTC	HV/MV OLTC
$\dot{\lambda}^{S}$ (€)	10000	-	-
$\dot{\lambda}^{O}$ (€)	-	20000	-
$\ddot{\lambda}^{S}$ (€/kWh)	400	-	-
$\ddot{\lambda}^{O}$ (€/kVA)	-	20	-
$\ddot{\lambda}^{\ddot{O}}$ (€/tap)	-	0.043	0.043
λ^{E} (€/kWh)	wholesale prices	-	-
Lifetime	10 years	30 years	-

The parameters defining energy storage systems and OLTC transformers are shown in Table 3 and Table 4. Technology degradation is not considered in this paper.

Table 3. Parameters of the OLTC transformers.

	$\underline{\varphi}$ (p.u.)	$\overline{\varphi}$ (p.u.)	$\bar{\phi}$	$\Delta\varphi$ (p.u.)	$\Delta\alpha$ (p.u.)
HV/MV OLTC	0.9	1.1	11	0.02	[0.02, … ,0.2]
MV/LV OLTC	0.95	1.05	5	0.025	[0.025, … ,0.1]

Table 4. Parameters of the energy storage systems.

	η^{+},η^{-}	γ	$\underline{\beta^{S}}\ (kWh)$	$\overline{\beta^{S}}(kWh)$	ς	ρ	ψ
Energy storage	0.97	0.01	100	200000	0.1	0.3	1

6. Results

6.1. Identification of candidate buses for placing energy storage devices and on-load tap changer transformers

Table 5 presents the candidate buses for placing MV/LV OLTC transformers and energy storage devices. The number of candidate buses is reduced but is still much higher than the final number of buses with placed technologies (see Figure 8).

Table 5. Candidate buses to place MV/LV OLTC transformers and energy storage devices.

	Scenario 1	Scenario 2
Buses selected by the heuristic algorithm	[69, 76]	[47, 53], 61
Buses manually selected by the DSO	10, 35, 110	10, 35, 71, 110
Nº of candidates	11	12

Figure 6 presents the voltage violations identified in scenario 1. The voltage violations were identified by the heuristic algorithm. The integration of EVs generates undervoltages in Area 2 (see Figure 4). The bus 76 presents the lowest voltage value (0.84 p.u.) and the highest number of undervoltages (78).

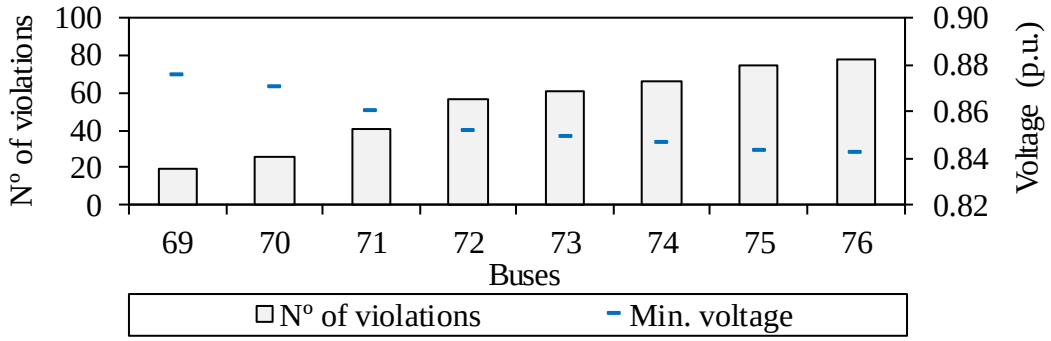

Figure 6. Voltage violations identified in scenario 1.

Figure 7 presents the voltage violations identified in scenario 2. The integration of PVs generates overvoltages in Area 1. The bus 76 presents the highest voltage value (1.13 p.u.) and the highest number of overvoltages (7).

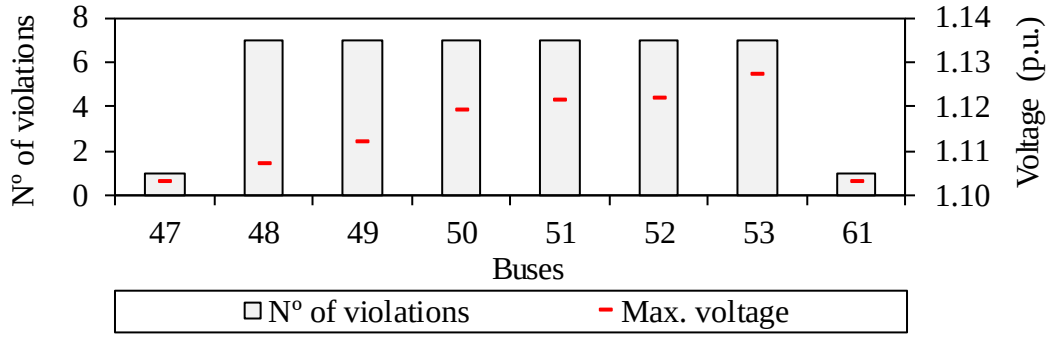

Figure 7. Voltage violations identified in scenario 2.

6.2. Identification of the critical-days and design-days

The critical-days and design-days model the period of 1 year. Table 6 shows the critical-days identified by the heuristic algorithm for scenarios 1 and 2. The design-days

are average hourly profiles computed based on the time series of 1 year. The weight W_t of each critical-day and design-day is also presented in Table 6.

Table 6. Critical-days and design-days for scenarios 1 and 2.

	Critical-days	Design-days
Scenario 1	January 7th ($W_t = 1$)	1 winter day ($W_t = 89$) 1 spring day ($W_t = 92$) 1 summer day ($W_t = 94$) 1 autumn day ($W_t = 89$)
Scenario 2	July 20th ($W_t = 1$)	1 winter day ($W_t = 90$) 1 spring day ($W_t = 92$) 1 summer day ($W_t = 93$) 1 autumn day ($W_t = 89$)

6.3. Joint versus individual optimization of technologies

This section compares the joint optimization of energy storage devices and MV/LV OLTC transformers to the individual optimization of each technology. Three possibilities are considered:

1. **joint optimization** of energy storage devices and MV/LV OLTC transformers (named joint);
2. **individual optimization** of energy storage devices (named individual 1);
3. **individual optimization** of MV/LV OLTC transformers (named individual 2).

Scenario 2 is used to perform this analysis.

6.3.1. Optimal sizing and placement of technologies

Figure 8 presents the location and size of the MV/LV OLTC transformers and energy storage devices. The three possible combinations of technologies solve the overvoltage problems detected in scenario 2.

The individual 2 placed 6 MV/LV OLTC transformers. This suggests that the joint optimization of the tap positions in both HV/MV and MV/LV OLTC transformers is enough to mitigate all overvoltage problems. The size of the transformers in buses 49, 51 and 52 was unmodified, while transformers in buses 48, 50 and 53 were replaced by larger OLTC transformers.

The individual 1 placed 2 energy storage devices. The energy storage in bus 53 has 309 kWh of capacity, 103 kWh of maximum active power and 103 kVAR of maximum reactive power. The energy storage device in bus 71 has 124 kWh of capacity, 41 kWh of maximum active power and 41 kVAR of maximum reactive power. The energy storage devices together with the HV/MV OLTC transformer regulate the voltage. The energy storage devices exploit the volt/VAR compensation functionality enabled by the power electronic converter to regulate voltage.

The joint optimization placed 1 MV/LV OLTC transformer and 1 storage device. The transformer of bus 53 was replaced by a larger OLTC transformer. The energy storage has 124 kWh of capacity, 41 kW of maximum active power and 41 kVAR of maximum reactive power.

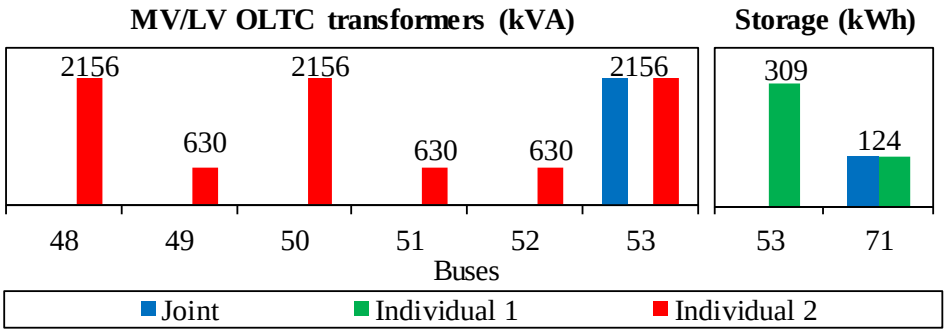

Figure 8. Location and size of the MV/LV OLTC transformers and energy storage devices in scenario 2.

6.3.2. Annual investment and operation net costs

Table 7 shows the annual investment and operation net costs for the three combinations of technologies. Positive values are costs and negative values are revenues.

The joint optimization presents the lowest total annual investment and operation cost of 197.1 k€ followed by individual 2 and individual 1 with total annual costs of 198.2 k€ and 204.8 k€. In addition, the joint optimization presents the cheapest investment planning strategy of 8.1 k€. Therefore, the joint optimization of technologies produces a more affordable planning strategy than the individual optimization of the technologies.

Table 7. Annual investment costs and operation net costs for scenario 2.

Type of cost	Cost terms	Joint	Individual 1	Individual 2
Investment (k€)	Energy storage	6.0	19.3	0
	MV/LV OLTC	2.1	0	9.6
Operation (k€)	Energy losses	189.3	186.5	188.4
	Energy storage	-0.4	-1.2	0
	MV/LV OLTC	~ 0	0	~ 0
	HV/MV OLTC	0.1	0.1	0.1
Total (k€)		197.1	204.8	198.2

The individual 1 presents the lowest annual operation cost of 185.5 k€ followed by individual 2 and joint optimization with annual operation costs of 188.6 k€ and 189.0 k€. The deployment of energy storage devices generates revenues through arbitrage and consequently reduces operating costs. However, investing only in energy storage is expensive and not cost-effective at current prices. Nonetheless, the expected reduction of the prices promises to turn energy storage into a very competitive technology.

6.4. Operation of the energy storage device and on-load tap changer transformers

The optimization model emulates the operation of the energy storage devices and OLTC transformers in order to evaluate the economic and technical viability of deploying and operating these technologies. This section analyzes the operation of the energy storage and OLTC transformers optimized by the joint approach in scenario 2.

6.4.1. Energy storage device

Figure 9 describes the operation of the energy storage device during the critical day. The energy storage device installed at bus 71 injects reactive power throughout the day

to increase the voltage in Area 2 (includes buses 62-112, see Figure 4). The objectives are two. The first objective is to reduce energy losses. The second is to maintain the voltages of Area 2 above 0.9 p.u. when the HV/MV OLTC transformer moves the tap down to compensate the high voltage values observed in Area 1 (see Figure 11). In addition, the energy storage device absorbs active power at 2nd and 3rd hours and injects active power at 18th and 19th hours in order to profit from price arbitrage. In the Iberian market. the wholesale prices are typically low in the early hours of the day and high at evening [32,33].

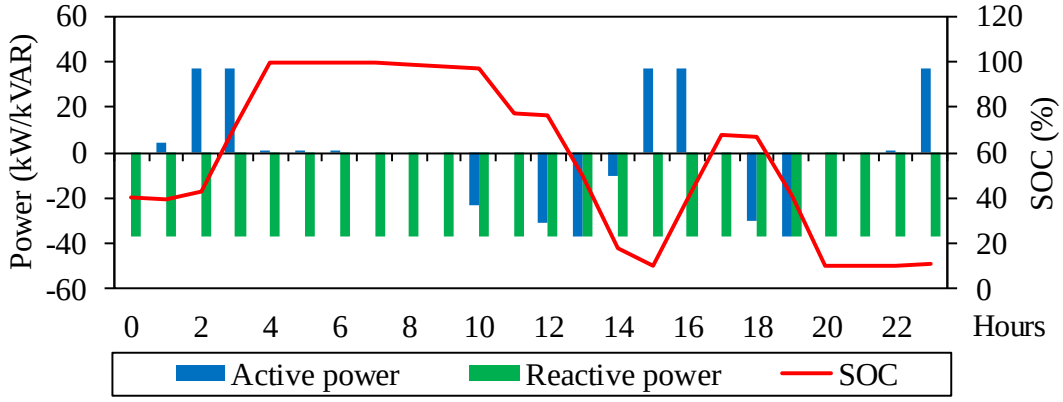

Figure 9. Operation of the energy storage device during the critical-day. Positive power values mean charging/absorbing. Negative power values mean discharging/injecting.

6.4.2. On-load tap changer transformers

Figure 10 and Figure 11 describe the operation of the MV/LV and HV/MV OLTC transformers along the critical day. The MV/LV OLTC transformer installed at bus 53 maintains the same tap position of 0.95 p.u. along the day, in order to keep the voltage on the LV side of the transformer within the technical limits. On the other hand, the HV/MV OLTC transformer moves the tap up and down according to the voltage conditions of the network. At 12th and 13th hours, the HV/MV OLTC transformer moves down the tap to 0.96 p.u., in order to keep the voltages of buses 47-53 and 61 below 1.1 p.u. This behavior is coordinated with the operation of the energy storage device. At the same hours, the energy storage injects active and reactive power to increase and keep the voltages of Area 2 above 0.9 p.u.

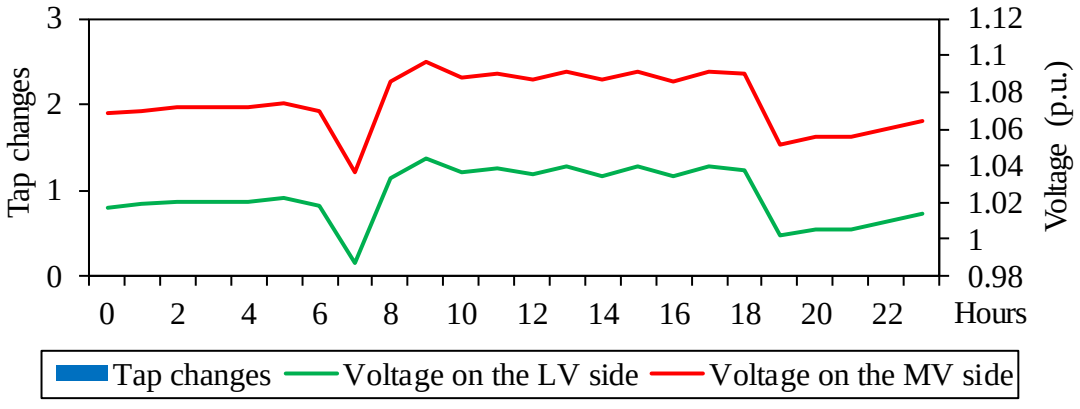

Figure 10. Operation of the MV/LV OLTC transformer during the critical-day.

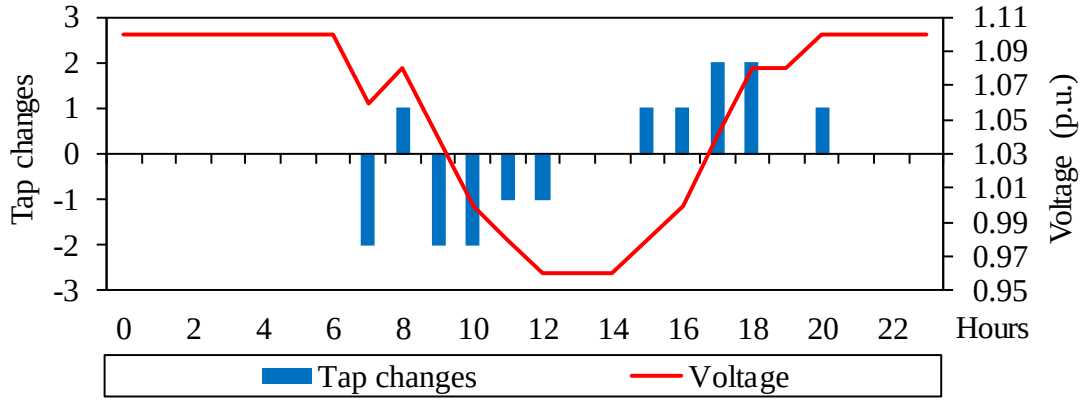

Figure 11. Operation of the HV/MV OLTC transformer during the critical-day. Positive and negative tap changes represent the movement of the tap in the positive (up) and negative (down) directions, respectively.

Figure 12 shows that the coordinated operation of the energy storage device with the OLTC transformers keeps the voltages of Area 1 (buses 1-61) below 1.1 p.u. and the voltages of Area 2 (buses 62-117) above 0.9 p.u. during the hours of high integration of PV generation (i.e., between the 9th and 17th hours). In the remaining hours of the day, the distribution network is operated at high voltages to reduce energy losses. The HV/MV OLTC transformer sets the voltage at slack bus equal to 1.1 p.u., as shown in Figure 11.

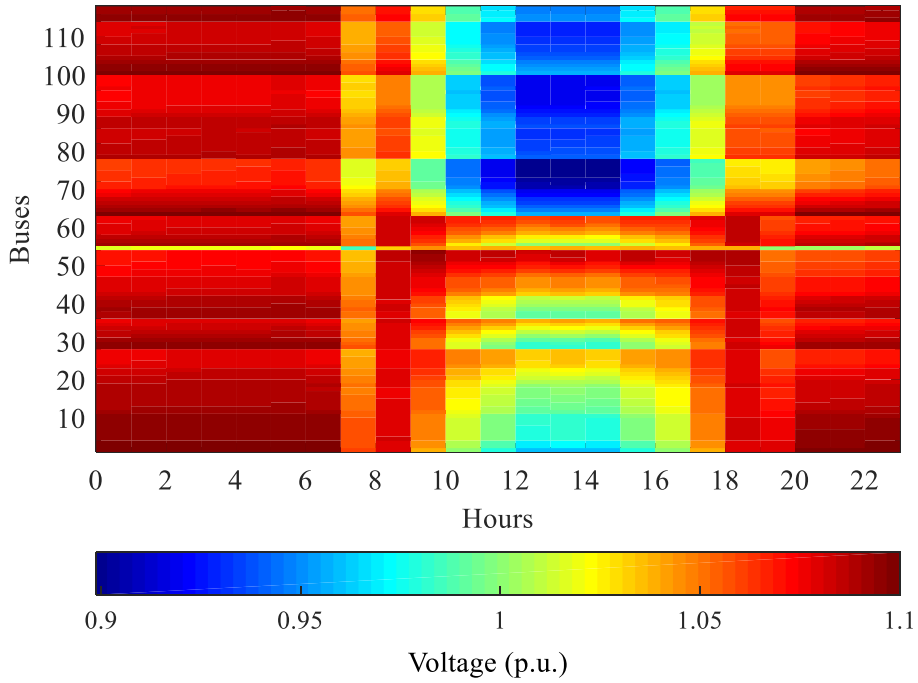

Figure 12. Voltages during the critical-day.

6.5. Constrained SOCP-OPF versus LinDistFlow

This section compares the proposed optimization model based on the constrained SOCP-OPF to the *LinDistFlow* formulation of the problem. Scenario 1 is used to perform this analysis.

6.5.1. Optimal sizing and placement of technologies

Figure 13 presents the location and size of the MV/LV OLTC transformers and energy storage devices. The constrained SOCP-OPF placed 8 MV/LV OLTC transformers and 1 energy storage device. The transformers of buses 70-71 and 73-76 maintained the same size, while the transformers of buses 69 and 72 were replaced by larger OLTC transformers. The energy storage selected in this scenario has 284 kWh of capacity, 95 kW of maximum active power and 95 kVAR of maximum reactive power. Energy storage is included in the solution as OLTC transformers. OLTC transformers only solve nodal voltage problems, while energy storage improves voltage profiles across different buses. The *LinDistFlow* formulation placed only MV/LV OLTC transformers.

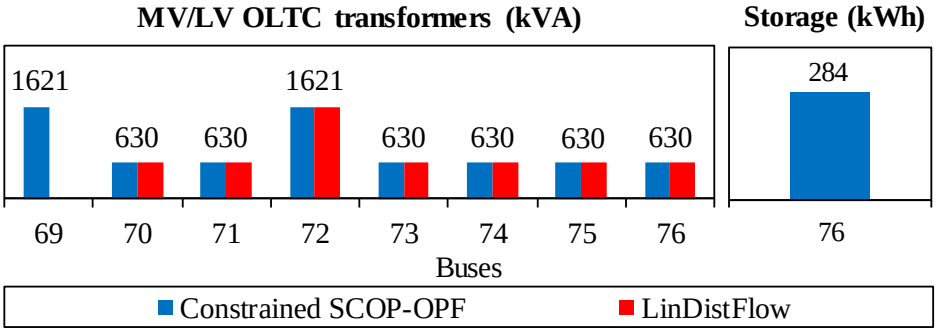

Figure 13. Location and size of the MV/LV OLTC transformers and energy storage devices in scenario 1.

6.5.2. Physical meaning of solutions

The *LinDistFlow* formulation places fewer technologies than the SOCP-OPF, which results in lower investment costs, as demonstrated in the next subsection. However, the *LinDistFlow* formulation may compute infeasible solutions, i.e. solutions that do not solve voltage problems, as shown in Figure 14. These undervoltage violations were verified after the deployment of the technologies with the *LinDistFlow*.

The SOCP-OPF only computes solutions with physical meaning, even for scenarios with reverse power flows. The deployment of the energy storage device in bus 76 produced reverse power flows in lines 73-74, 74-75 and 75-76.

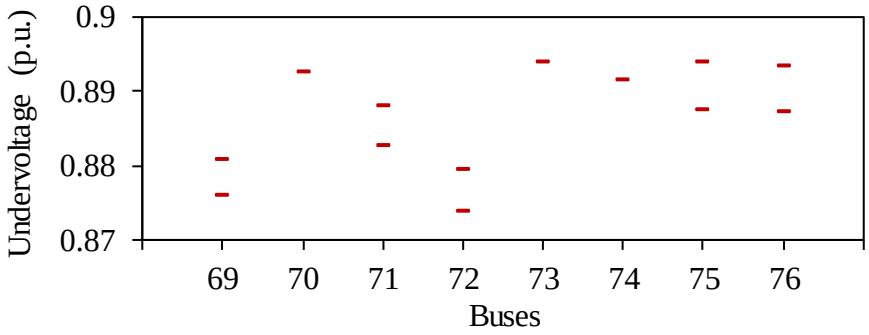

Figure 14. Voltage violations after technology deployment with the *LinDistFlow*.

6.5.3. Annual investment and operation net costs

The planning solution of the constrained SOCP-OPF is feasible and presents an annual investment cost of 22.3 k€. The *LinDistFlow* formulation presents the lowest annual investment cost of 8.3 k€. However, the planning strategy is infeasible since the solutions violate the voltage limits. Table 8 shows the annual investment and operation net costs. Positive values are costs and negative values are revenues.

Table 8. Annual investment and operation net costs for scenario 1.

Type of cost	Cost terms	Constrained SOCP-OPF	*LinDistFlow*
Investment (k€)	Energy storage	12.3	0
	MV/LV OLTC	10.0	8.3
Operation (k€)	Energy storage	-0.8	0
	MV/LV OLTC	0.4	~ 0
	HV/MV OLTC	~ 0	~ 0
Total (k€)		21.9	8.3

6.5.4. Computational performance

The optimization models based on the constrained SOCP-OPF and *LinDistFlow* formulation were implemented in Python and solved by the IBM CPLEX 12.7 optimizer on a machine with 256 GB RAM and an Intel(R) Xeon(R) CPU E7-4820 CPU clocked at 2.0 GHz. The size and execution time of the resulting optimization problems are presented in Table 9. Numerical results show fast execution times for the size and complexity of the planning problems.

Table 9. Size of the problems and execution times.

	Constrained SOCP-OPF	*LinDistFlow*
Continuous variables	118,110	61,830
Binary variables	5,059	5,059
Linear constraints	165,327	122,127
Quadratic constraints	14,040	0
Execution time	2.9 h	9.8 min

7. Conclusion

The widespread integration of distributed energy resources will produce reverse power flows, overvoltage and undervoltage problems in the distribution grids. This paper proposes a new optimization model to plan MV distribution networks characterized by a high integration of distributed energy resources. The optimization model defines the optimal mix, size, and placement of energy storage devices and MV/LV OLTC transformers with the objectives of mitigating network technical problems and minimizing both operation and investment costs.

The proposed optimization model based on the constrained SOCP-OPF computes only feasible solutions with physical meaning, even for extreme scenarios of operation characterized by overvoltages and undervoltages. Conversely, the *LinDistFlow* formulation produces infeasible solutions in scenarios with undervoltage problems. Both approaches present reasonable execution times compatible with real-scale distribution networks. This shows that the proposed methodology for sitting and sizing is applicable to real-size grids with significant improvements in accuracy when compared to linearized approaches.

The numerical results show that the joint optimization of energy storage devices and MV/LV OLTC transformers produces a more affordable planning strategy than the individual optimization of the technologies. Both technologies are capable of regulating the voltage. For this purpose, the OLTC is a more cost-effective technology at the current prices. However, the consideration of other additional services, such as arbitrage,

frequency regulation, and congestion management may turn the energy storage in a very competitive technology.

Future work consists of incorporating additional features in the planning problem, such as technology degradation and network reconfiguration.

Acknowledgments

The authors of this publication would like to acknowledge Dan Ton and Ali Ghassemian, Program Managers at the U.S. Department of Energy, for the support granted to this work through the Microgrid R&D Program and the Advanced Grid Modeling Program. The work of José Iria was also supported by Fundação para a Ciência e Tecnologia with the Ph.D. Scholarship PD/BD/113716/2015.

References

[1] H. Pandžić, Y. Dvorkin, M. Carrión, Investments in merchant energy storage: Trading-off between energy and reserve markets, Applied Energy. 230 (2018) 277–286. doi:10.1016/j.apenergy.2018.08.088.

[2] Y. Dvorkin, R. Fernandez-Blanco, D.S. Kirschen, H. Pandzic, J.P. Watson, C.A. Silva-Monroy, Ensuring Profitability of Energy Storage, IEEE Transactions on Power Systems. 32 (2017) 611–623. doi:10.1109/TPWRS.2016.2563259.

[3] M. Stadler, G. Cardoso, S. Mashayekh, T. Forget, N. DeForest, A. Agarwal, A. Schönbein, Value streams in microgrids: A literature review, Applied Energy. 162 (2016) 980–989. doi:10.1016/j.apenergy.2015.10.081.

[4] S. Wen, H. Lan, Q. Fu, D.C. Yu, L. Zhang, Economic allocation for energy storage system considering wind power distribution, IEEE Transactions on Power Systems. 30 (2015) 644–652. doi:10.1109/TPWRS.2014.2337936.

[5] S.W. Alnaser, L.F. Ochoa, Optimal Sizing and Control of Energy Storage in Wind Power-Rich Distribution Networks, IEEE Transactions on Power Systems. 31 (2016) 2004–2013. doi:10.1109/TPWRS.2015.2465181.

[6] S. Mashayekh, M. Stadler, G. Cardoso, M. Heleno, A mixed integer linear programming approach for optimal DER portfolio, sizing, and placement in multi-energy microgrids, Applied Energy. 187 (2017) 154–168. doi:10.1016/j.apenergy.2016.11.020.

[7] G. Cardoso, T. Brouhard, N. DeForest, D. Wang, M. Heleno, L. Kotzur, Battery aging in multi-energy microgrid design using mixed integer linear programming, Applied Energy. 231 (2018) 1059–1069. doi:10.1016/j.apenergy.2018.09.185.

[8] S. Mashayekh, M. Stadler, G. Cardoso, M. Heleno, S. Chalil Madathil, H. Nagarajan, R. Bent, M. Mueller-Stoffels, X. Lu, J. Wang, Security-Constrained Design of Isolated Multi-Energy Microgrids, IEEE Transactions on Power Systems. 8950 (2017) 1–11. doi:10.1109/TPWRS.2017.2748060.

[9] Y. Yang, H. Li, A. Aichhorn, J. Zheng, M. Greenleaf, Sizing strategy of distributed battery storage system with high penetration of photovoltaic for voltage regulation and peak load shaving, IEEE Transactions on Smart Grid. 5 (2014) 982–991. doi:10.1109/TSG.2013.2282504.

[10] M. Nick, R. Cherkaoui, M. Paolone, Optimal allocation of dispersed energy storage systems in active distribution networks for energy balance and grid support, IEEE Transactions on Power Systems. 29 (2014) 2300–2310. doi:10.1109/TPWRS.2014.2302020.

[11] A.R. Camargo, C.A. Castro, M. Lavorato, Optimal allocation of energy storage devices in distribution systems considering lifetime characteristics of batteries, in:

2016 IEEE International Conference on Power System Technology (POWERCON), IEEE, 2016: pp. 1–6. doi:10.1109/POWERCON.2016.7753965.
[12] Y. Tang, S.H. Low, Optimal Placement of Energy Storage in Distribution Networks, IEEE Transactions on Smart Grid. 8 (2017) 3094–3103. doi:10.1109/TSG.2017.2711921.
[13] X. Shen, M. Shahidehpour, Y. Han, S. Zhu, J. Zheng, Expansion Planning of Active Distribution Networks With Centralized and Distributed Energy Storage Systems, IEEE Transactions on Sustainable Energy. 8 (2017) 126–134. doi:10.1109/TSTE.2016.2586027.
[14] A. Hassan, Y. Dvorkin, Energy Storage Siting and Sizing in Coordinated Distribution and Transmission Systems, IEEE Transactions on Sustainable Energy. 9 (2018) 1692–1701. doi:10.1109/TSTE.2018.2809580.
[15] E. Grover-Silva, R. Girard, G. Kariniotakis, Optimal sizing and placement of distribution grid connected battery systems through an SOCP optimal power flow algorithm, Applied Energy. 219 (2018) 385–393. doi:10.1016/j.apenergy.2017.09.008.
[16] S.Y. Abdelouadoud, R. Girard, F.P. Neirac, T. Guiot, Optimal power flow of a distribution system based on increasingly tight cutting planes added to a second order cone relaxation, International Journal of Electrical Power and Energy Systems. 69 (2015) 9–17. doi:10.1016/j.ijepes.2014.12.084.
[17] C. Wang, G. Song, P. Li, H. Ji, J. Zhao, J. Wu, Optimal siting and sizing of soft open points in active electrical distribution networks, Applied Energy. 189 (2017) 301–309. doi:10.1016/j.apenergy.2016.12.075.
[18] A. Zakariazadeh, O. Homaee, S. Jadid, P. Siano, A new approach for real time voltage control using demand response in an automated distribution system, Applied Energy. 117 (2014) 157–166. doi:10.1016/j.apenergy.2013.12.004.
[19] J.L. Meirinhos, D.E. Rua, L.M. Carvalho, A.G. Madureira, Multi-temporal Optimal Power Flow for voltage control in MV networks using Distributed Energy Resources, Electric Power Systems Research. 146 (2017) 25–32. doi:10.1016/j.epsr.2017.01.016.
[20] M. Armendáriz, K. Paridari, E. Wallin, L. Nordström, Comparative study of optimal controller placement considering uncertainty in PV growth and distribution grid expansion, Electric Power Systems Research. 155 (2018) 48–57. doi:10.1016/j.epsr.2017.10.001.
[21] M. Armendáriz, M. Heleno, G. Cardoso, S. Mashayekh, M. Stadler, L. Nordström, Coordinated microgrid investment and planning process considering the system operator, Applied Energy. 200 (2017) 132–140. doi:10.1016/j.apenergy.2017.05.076.
[22] H. Hosseinpour, B. Bastaee, Optimal placement of on-load tap changers in distribution networks using SA-TLBO method, International Journal of Electrical Power and Energy Systems. 64 (2015) 1119–1128. doi:10.1016/j.ijepes.2014.09.009.
[23] S. Xie, Z. Hu, D. Zhou, Y. Li, S. Kong, W. Lin, Y. Zheng, Multi-objective active distribution networks expansion planning by scenario-based stochastic programming considering uncertain and random weight of network, Applied Energy. 219 (2018) 207–225. doi:10.1016/j.apenergy.2018.03.023.
[24] M.E. Baran, F.F. Wu, Network reconfiguration in distribution systems for loss reduction and load balancing, Power Delivery, IEEE Transactions On. 4 (1989) 1401–1407. doi:10.1109/61.25627.
[25] L. Gan, N. Li, U. Topcu, S.H. Low, Exact Convex Relaxation of Optimal Power

Flow in Radial Networks, IEEE Transactions on Automatic Control. 60 (2015) 72–87. doi:10.1109/TAC.2014.2332712.
[26] D. Zhang, Z. Fu, L. Zhang, An improved TS algorithm for loss-minimum reconfiguration in large-scale distribution systems, Electric Power Systems Research. 77 (2007) 685–694. doi:10.1016/j.epsr.2006.06.005.
[27] F.J. Soares, J.A.P. Lopes, P.M.R. Almeida, A stochastic model to simulate electric vehicles motion and quantify the energy required from the grid, in: 2011 17th Power Systems Computation Conference (PSCC), 2011: pp. 22–26. http://www.pscc-central.org/uploads/tx_ethpublications/fp359.pdf.
[28] J. Iria, F. Soares, A cluster-based optimization approach to support the participation of an aggregator of a larger number of prosumers in the day-ahead energy market, Electric Power Systems Research. 168 (2019) 324–335. doi:10.1016/j.epsr.2018.11.022.
[29] M. Nijhuis, M. Gibescu, J.F.G. Cobben, Incorporation of on-load tap changer transformers in low-voltage network planning, IEEE PES Innovative Smart Grid Technologies Conference Europe. (2017). doi:10.1109/ISGTEurope.2016.7856207.
[30] European Network of Transmission System Operators for Electricity (ENTSO-E), ENTSO-E Transparency Platform, (n.d.). https://transparency.entsoe.eu/ (accessed October 28, 2016).
[31] L. Hirth, J. Mühlenpfordt, M. Bulkeley, The ENTSO-E Transparency Platform – A review of Europe's most ambitious electricity data platform, Applied Energy. 225 (2018) 1054–1067. doi:10.1016/j.apenergy.2018.04.048.
[32] J. Iria, F. Soares, M. Matos, Optimal bidding strategy for an aggregator of prosumers in energy and secondary reserve markets, Applied Energy. 238 (2019) 1361–1372. doi:10.1016/j.apenergy.2019.01.191.
[33] J. Iria, F. Soares, M. Matos, Optimal supply and demand bidding strategy for an aggregator of small prosumers, Applied Energy. 213 (2018) 658–669. doi:10.1016/j.apenergy.2017.09.002.